Supporting Information for

Efficient Electrochemical Transformation of CO_2 to C_2/C_3 Chemicals on Benzimidazole-Functionalized Copper Surfaces

Shenghong Zhong[a†], Xiulin Yang[a†], Zhen Cao[a†], Xinglong Dong[a], Sergey M. Kozlov[a], Laura Falivene[a], Jing-Kai Huang[a], Xiaofeng Zhou[a], Mohamed N. Hedhili[b], Zhiping Lai[a], Kuo-Wei Huang[a], Yu Han[a*], Luigi Cavallo[a*], and Lain-Jong Li[a*]

[a.] Physical Science and Engineering Division, King Abdullah University of Science and Technology (KAUST), Thuwal 23955-6900, Kingdom of Saudi Arabia

[b.] Imaging and Characterization Laboratory, King Abdullah University of Science and Technology (KAUST), Thuwal 23955-6900, Kingdom of Saudi Arabia

Experimental Details

Catalyst preparation

Commercial Cu foils (Sigma-Aldrich, 99.98%) were first cleaned with ethanol (or propan-2-ol) and deionized water (18.2 MΩ/cm) and then electro-chemically treated in 0.3M KCl (Sigma-Aldrich, 99.0%) solution with five cyclic voltammogram (CV) scans ranging from 0.5 to -1.5 V (vs. Ag/AgCl, without IR compensation) at a rate of 20 mV/s. Ligands (benzimidazole, 2-methylimidazole and 2-imidazolecarboxaldehyde) modified copper foils were prepared by simply soaking the pre-treated Cu foils in ligands ethanol (or propan-2-ol) solution (10 mL, 50 mM) for 2 days, and then rinsed with ethanol (or propan-2-ol), deionized water and dried under ambient condition for at least 1 day prior to utilization.

Pristine Cu foils were prepared by first mechanically polishing using a sandpaper and then electropolishing in phosphoric acid (85% in H_2O, Aldrich) at 2.1 V vs. a graphite rod counter electrode placed at a distance of 1.5 cm for 5 mins.

Catalyst characterization

The morphology of the samples was observed by an FEI Nova Nano 630 Scanning Electron Microscopy (SEM). X-ray photoelectron spectroscopy (XPS) was conducted using a Kratos Axis Ultra DLD spectrometer equipped with a monochromatic Al Kα X-ray source (hv=1486.6 eV) operating at 150W, a multi- channel plate and delay line detector under a vacuum of $1*10^{-9}$ mbar. The survey and high-resolution spectra were collected at fixed analyzer pass energies of 160 and 20 eV, respectively. Binding energies were referenced to the C1s speak (set at 284.5 eV) of the sp2 hybridized carbon from ligands, while for bare copper foils C1s peak was set at 284.8 eV (sp3 hybridized carbon). The Raman spectra were acquired using a 532-nm laser with a confocal microscope system (WITec Alpha300). UV-vis spectrum was collected with a spectrophotometer (Shimadazu, UV 2550). FTIR spectra were recorded by a Nicolet iS10 FTIR spectrometer.

Electrochemically active surface areas (ECSAs) were determined by measuring double layer capacitances using cyclic voltammetry (CV) method. CV experiments were performed in the same electrochemical cell after electrochemically reduction of CO_2 in CO_2-saturated 0.1M $KHCO_3$ solution at -2 V (vs. Ag/AgCl, without IR compensation). CV curves were obtained within a potential range in which no faradaic processes were occurring (+0.53V~+0.45 V for Cu(BIM)x-modified Cu foil, and +0.45 V~+0.35V for bare Cu foil, vs. RHE), and the geometric current density was plotted against the scan rate of the CV. The slope of the linear regression gives the capacitance.

Catalytic evaluation

All the electrochemical experiments were carried out in an air-tight, glass frit-separated two-compartment three-electrode electrochemical cell using a Biologic VMP-300 potentiostat. Applied potentials are reported as RHE potentials scale, unless otherwise stated. Prior to reaction, the catalyst was electro-treated under -2 V (vs. Ag/AgCl, without IR conpensation) in CO_2-saturated 0.1 M $KHCO_3$ solution until reach a stable current density to activate the catalyst and also to remove the potential ethanol residue. During the electrochemical reduction (for isotopic labeling experiment, 0.1 M $KH^{13}CO_3$ electrolyte was prepared by bubbling $^{13}CO_2$ into 0.1 M KOH (Sigma-Aldrich, 85%) until its pH reaching 6.8), as prepared catalysts were used as working electrode. A coiled platinum wire and an Ag/AgCl in saturated KCl were used as counter and reference electrodes, respectively. And CO_2 gas was continuously bubbled into the cathodic compartment at a rate of 10 mL/min. The eluent was delivered directly to the sampling loop of an on-line pre-calibrated gas chromatograph (Agilent 7890B) which was equipped with two TCD channels. The Faradaic efficiencies (FEs) of gaseous products were calculated from the volume concentration of gaseous products.

After 1 hour reduction, the liquid products were collected from electrolyte and analyzed using a Bruker AV-III 700MHz (or 950MHz) liquid H^1-NMR spectrometer. Small amount of dimethylsulfoxide (DMSO) (Sigma-Aldrich, 99.5%) in D_2O (Sigma-Aldrich, 99.9%) was sealed in a coaxial insert as an external reference. After calibration of the external reference with standard product solution, NMR tubes were then rinsed with deionized water and the collected electrolyte for three times. 500 μL solution were transferred into NMR tube for analysis. During the NMR analysis 64 cycles of scan were performed, and peaks shift were

recorded, peaks area (DMSO was always set as 1) were calculated as an index of their amount. Chemical shift was calibrated with a standard of 2.6 ppm of DMSO.

For stability test, to avoid the accumulation of carbonaceous species, electrolyte was refreshed every hour.

Computational Details

The calculations were performed using PBE[1] level of density functional theory (DFT), and the vdW interactions were described using the Grimme's dispersion correction[2]. The Valence electrons were described using 550 eV plane wave basis set and the interactions with the core electrons was treated using the projected augmented wave (PAW) technique[3]. The Gaussian smearing of 0.1 eV was applied to the occupation of electronic eigenstates. Slab calculations were performed using 3×3×1 k-point mesh. Geometry optimization was performed with the following criteria: forces acting on atoms should be smaller than 0.02 eV/nm. We used the following 6-layer slab with experimental lattice parameter[4]. Following the calculations performed by Goddard et al[5], we choose the Cu (100) surface to carry on the calculations.

As it is demonstrated in the previous simulations[5], CO_2RR on Cu (100) surface can proceed through both [HCOO]* and [COOH]* species. The critical factor determines the reaction path is if CO_2 reacted with adsorbed hydrogen (carries negative charges) or the hydrogen (carries positive charges) from $[H_3O]^+/H_2O$. Within the computational hydrogen electrode (CHE) framework[6], our calculations demonstrate the protonated Cu-BIMH is more stable if the applied voltage is below -0.71 V vs. RHE. The hydrogen in BIMH carries different Bader charges (Figure S13) compared with those hydrogen atoms absorbed onto the Cu surface: the former one carries positive partial charges, while the latter one carriers the negative partial charges. Therefore, hydrogen from both H_2O and BIMH can be proton source to hydrogenate the negatively charged O of CO_2 and form [COOH]*. Since [COOH]* is the precursor to form CO, this reaction path can lead to significant increment in CO formation. As it is reported in previous studies[7], the produced CO can further form C_2/C_3 species under applied voltage. Therefore, the increment in CO formation may be the reason in C_2/C_3 formation under working potential described in this work.

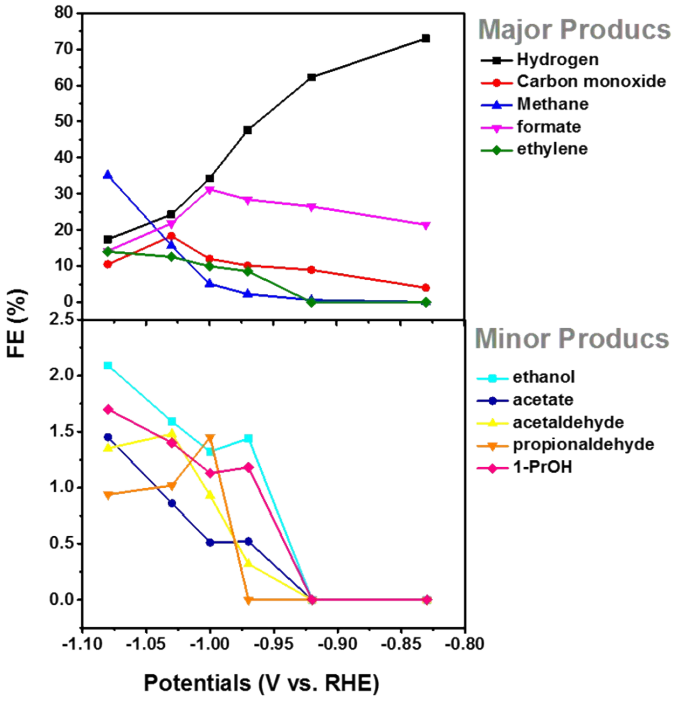

Figure S1 | CO_2RR performance of pristine Cu foil. Major products are hydrogen, carbon monoxide, methane, formate and ethylene, minor products include ethanol, acetate, acetaldehyde, propionaldehyde and 1-propanol. The reaction products distribution for the as-received Cu foil is close to previous reports by Jaramillo's group (Energy. Environ. Sci. 2012, 5, 7050).

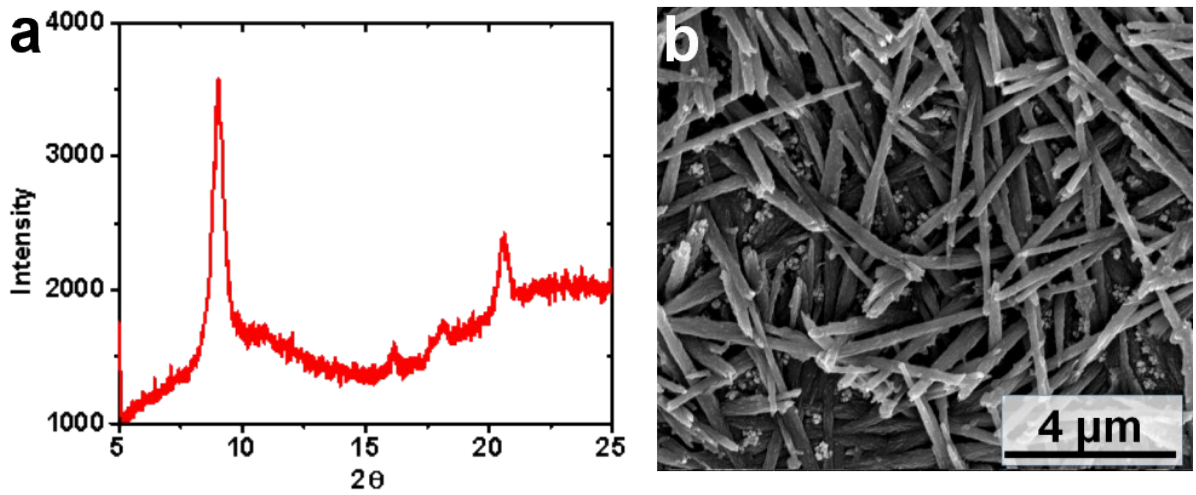

Figure S2 | a. Powder XRD analysis of Cu(BIM)$_x$. Cu(BIM)$_x$ was collected and purified by centrifugation (10000 RPM, 10 min) and dried in a vacuum oven (60°C). The experimental results prove the formation of Cu-ligands complex. **b**. SEM image of benzimidazole-modified Cu foil after 1 hour test of CO_2RR at -1.07 V vs. RHE.

Table S1 | FTIR peak assignment of Cu(BIM)$_x$ modified Cu foil. There is no N-H bond in FTIR spectrum of the Cu(BIM)$_x$ catalyst, which suggests the deprotonation of N-H during the formation of Cu(BIM)$_x$ complex. This is a strong support of the formation of Cu-N bond. Furthermore we can judge that both N atoms from benzimidazole are bonded to Cu atoms.

Observed wavenumber (cm^{-1})	**Assignment**
3123	(C-H) stretching
3077	(C-H) stretching
3046	(C-H) stretching
2926	(2*1467)
2853	(1467+1364)
1780	(C=O) stretching
1737	(C=O) stretching
1606	(C=C) stretching
1467	(C=C) stretching
1364	(C-N) stretching

1300	(C-N) stretching
1281	(C-H) in-plane bending
1239	(C-C) stretching
1202	(C-H) in-plane bending
1184	(C-H) in-plane bending
1148	(C-H) in-plane bending
1118	(C-H) in-plane bending
1002	(C-C-C) trigonal bending
921	(C-H) out-of-plane bending
906	(C-H) out-of-plane bending
875	(C-H) out-of-plane bending
776	(C-H) out-of-plane bending
745	(C-H) out-of-plane bending
640	(C-C-C) in-plane bending

Table S2 | Raman peak assignment for Cu(BIM)$_x$ modified Cu foil. Cu-N stretching peak is found at 462 cm^{-1},[8] which proves that benzimidazole and Cu react to form Cu-N bond.

Observed wavenumber (cm^{-1})	**Assignment**
777	(C-H) out-of-plane bending
654	(C-C-C) out-of-plane bending
582	(C-C-C) out-of-plane bending
553	(C-C-C) in-plane bending
462	(Cu-N) stretching
280	(Cu-O) stretching

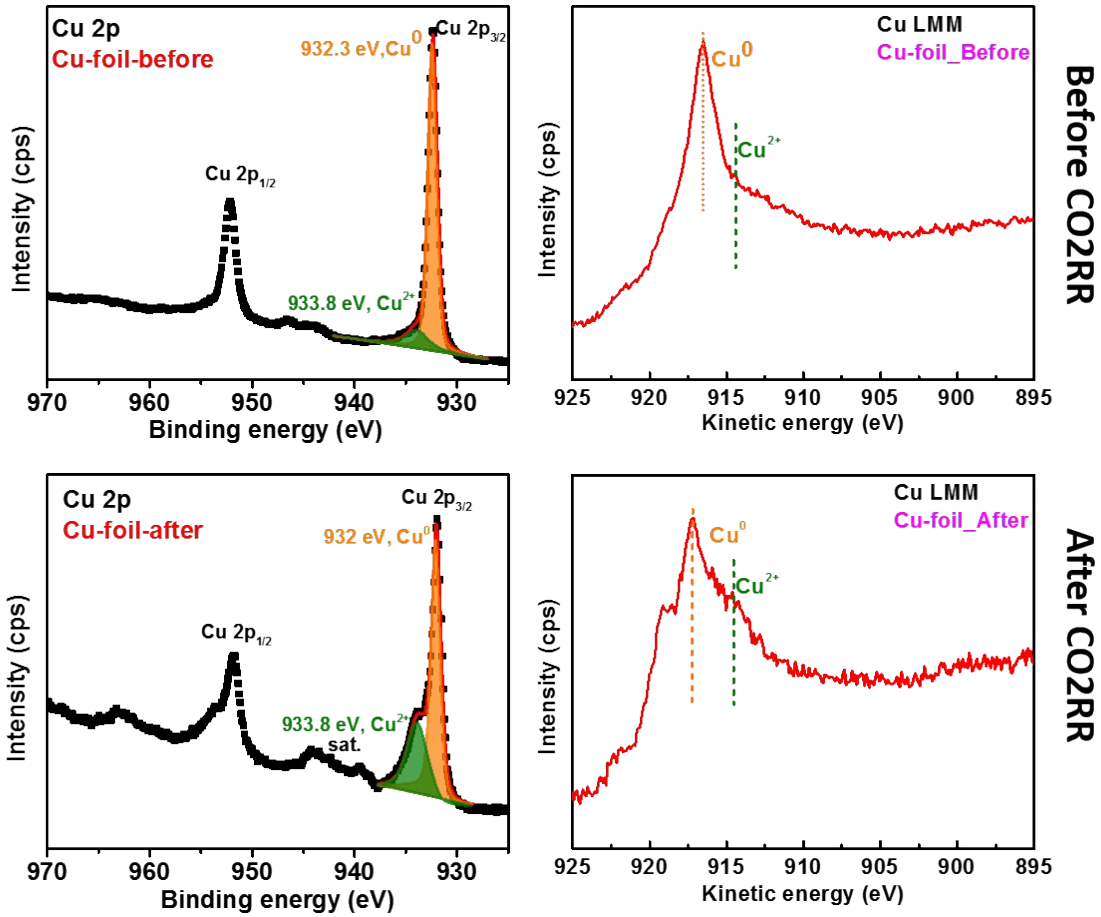

Figure S3 | High-resolution XPS Cu 2p and Cu LMM Auger spectra of bare Cu-foil before and after CO_2RR. Before and after CO_2RR, Cu^0 is the main species of copper foil. The small amount of Cu^{2+} was caused by surface oxidation in air when waiting for XPS measurements.

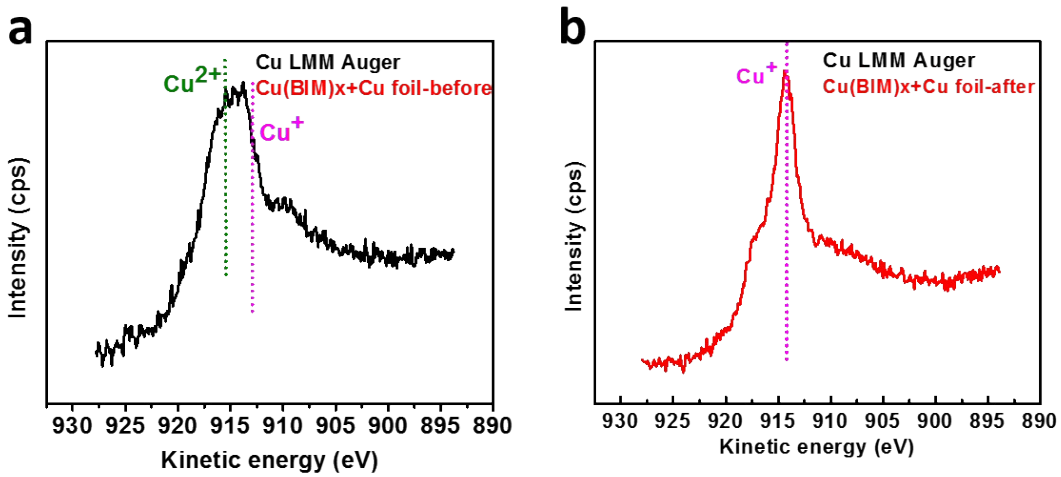

Figure S4 | Auger spectrum of Cu(BIM)$_x$ modified Cu foil before (a) and after (b) CO_2RR. Before CO_2RR Cu^{2+} and Cu^+ are the main species, however after CO_2RR, only Cu^+ is detectable, indicating that Cu^{2+} in the complexes may be reduced to Cu^+ under the negative voltage applied.

Table S3 | ^{1}H-NMR peak assignment of liquid products of CO_2RR

Chemical shift	^{1}H splitting	Assignment	
8.29	s	$HCOO^-$	Formate
3.86	septuple	$(CH_3)_2CHOH$	2-Propanol
3.50	q	CH_3CH_2OH	Ethanol
3.46	t	$CH_3CH_2CH_2CH_2OH$	n-Butanol
3.41	t	$CH_3CH_2CH_2OH$	n-Propanol
2.58	s	DMSO	external Standard
2.08	d	CH_3CHO	Acetaldehyde
1.76	s	CH_3COO^-	Acetate
1.39	sextet	$CH_3CH_2CH_2OH$	n-Propanol
1.37	pentadruple	$CH_3CH2CH_2CH_2OH$	n-Butanol
1.19	sextet	$CH_3CH_2CH_2CH_2OH$	n-Butanol
1.17	d	$CH_3CH(OH)_2$	Acetaldehyde
1.02	t	CH_3CH_2OH	Ethanol
1.01	d	$(CH_3)_2CHOH$	2-Propanol
0.89	t	CH_3CH_2CHO	Propionaldehyde
0.75	t	$CH_3CH_2CH_2CH_2OH$	n-Butanol
0.73	q	$CH_3CH_2CH_2OH$ & $CH_3CH_2CH(OH)_2$	n-Propanol Propionaldehyde

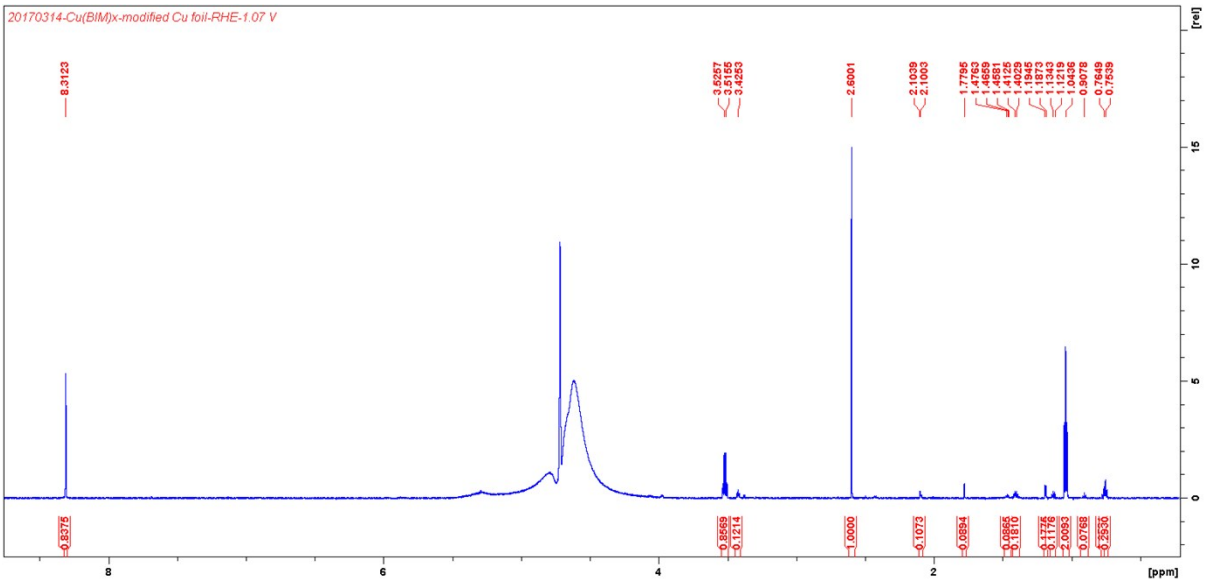

Figure S5 | One typical ^{1}H-NMR results of liquid products generated by Cu(BIM)$_x$ modified Cu foil catalyst at -1.07 V for 1 hour. The area of external reference DMSO (chemical shift 2.6 ppm)[9] was set as 1. Formate, ethanol, acetate, acetaldehyde, propionaldehyde and n-propanol were detected.

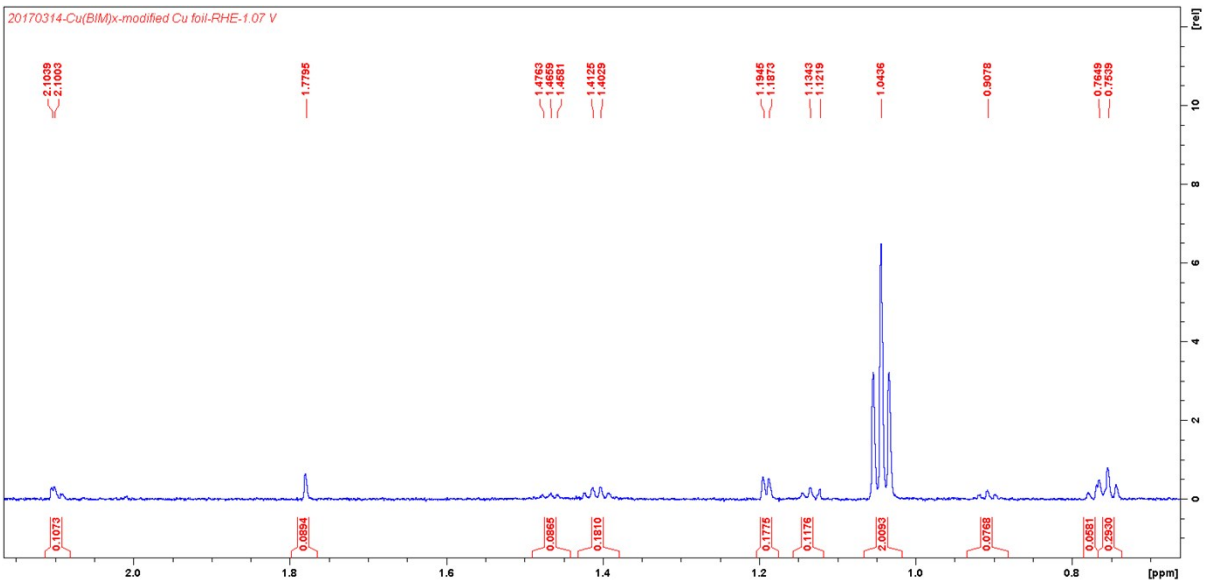

Figure S6 | Fine structure of ^{1}H-NMR peaks (ranging from 0.7 to 2.2 ppm). ^{1}H-splitting of the peaks were shown clearly. Please note that the quartet peak around 0.75 ppm were formed by the overlapping of two triple peaks of propionaldehyde and n-propanol.

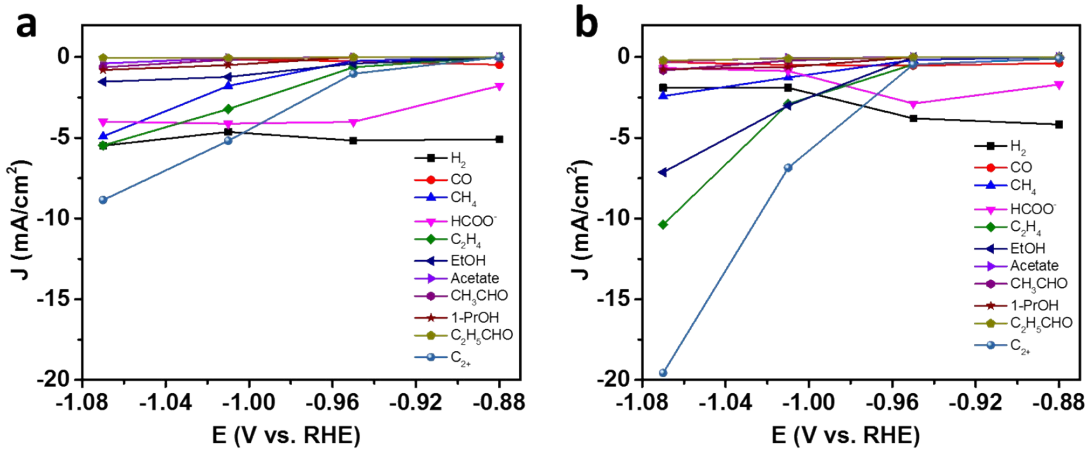

Figure S7 | Partial current density of all CO_2RR products and C_{2+} products of (a) bare Cu foil and (b) the benzimidazole-modified Cu foil under various working potentials

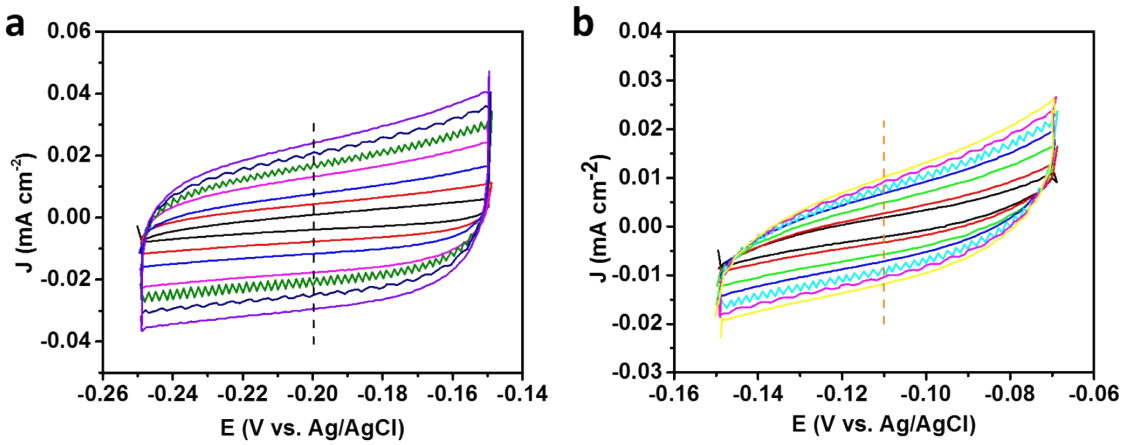

Figure S8 | CV curves at various scan rates of (a) bare Cu foil and (b) Cu(BIM)$_x$ modified Cu foil.

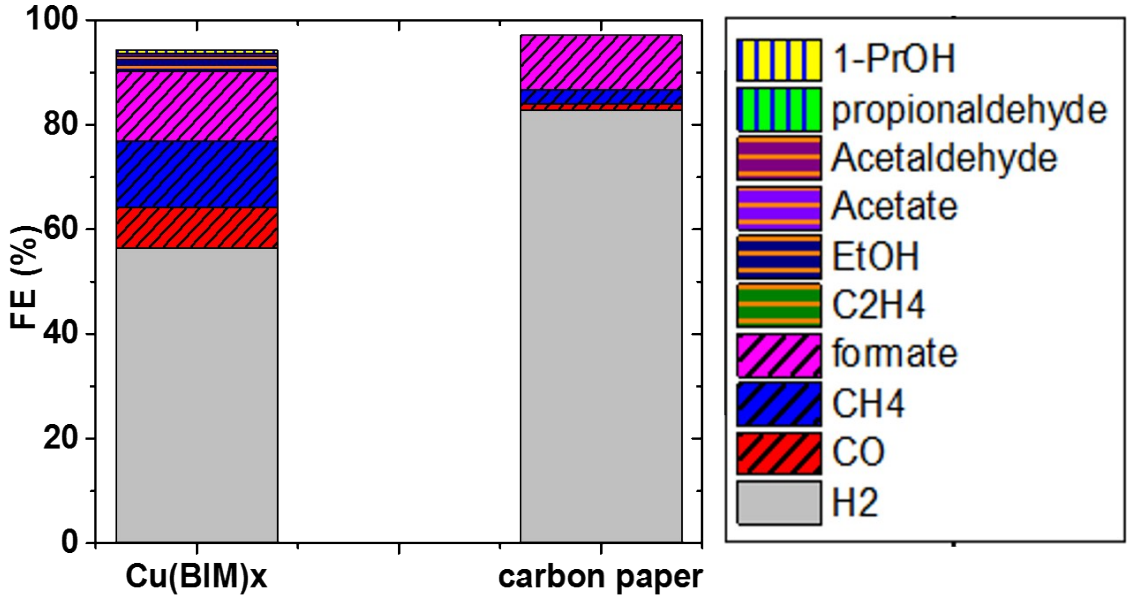

Figure S9 | CO_2RR performance of $Cu(BIM)_x$ complex at -1.1V (vs. RHE). $Cu(BIM)_x$ were drop-casted on carbon paper. The results show major products are C_0 and C_1 chemicals, proving that $Cu(BIM)_x$ complex is not the active site in $Cu(BIM)_x$-modified Cu foil catalysts. $Cu(BIM)_x$ functionalized carbon paper presents a higher FE of CO and CH_4 than bare carbon paper, which supports our proposed mechanism that $Cu(BIM)_x$ could provide $H^{\delta+}$ to boost the formation of CO.

Table S4 | Stability of each product of CO_2RR by Cu(BIM)$_x$-modified Cu foil at -1.09 V (vs. RHE)

Time (h)	FE (%)												
	C_0	C_1				C_2					C_3		
	H_2	CO	CH_4	formate	Sum	C_2H_4	EtOH	Acetate	Acetaldehyde	Sum	Propionaldehyde	1-PrOH	Sum
1	7.54	1.21	9.56	2.66	13.43	41.11	28.23	1.05	3.28	73.67	0.79	3.01	3.8
2	6.77	1.34	12.85	3.16	17.35	38.64	27.9	0.77	2.9	70.21	1.03	3.18	4.21
3	7.29	1.58	17.14	3.67	22.39	35.85	26.15	0.7	2.6	65.3	1.17	2.56	3.73
4	6.71	1.79	19.36	4.28	25.43	33.24	26.08	0.76	3.01	63.09	1.02	2.15	3.17
5	6.8	1.69	21.39	5.02	28.1	31.53	25.1	0.76	2.53	59.92	0.76	3.29	4.05
6	8.33	1.65	23.38	5.51	30.54	30.18	21.97	0.75	2.51	55.41	1.26	2.67	3.93
7	8.9	1.58	24.11	5.8	31.49	27.95	22.15	0.66	2.64	53.4	0.79	2.79	3.58
8	8.64	1.52	23.96	5.12	30.6	28.18	21.86	0.67	4.77	55.48	0.67	3.04	3.71
9	9.64	1.76	28.52	6.69	36.97	25.16	19.62	0.51	2.39	47.68	0.77	2.62	3.39
10	8.72	1.72	28.38	6.37	36.47	25.46	19.4	0.78	3.78	49.42	0.76	3.85	4.61

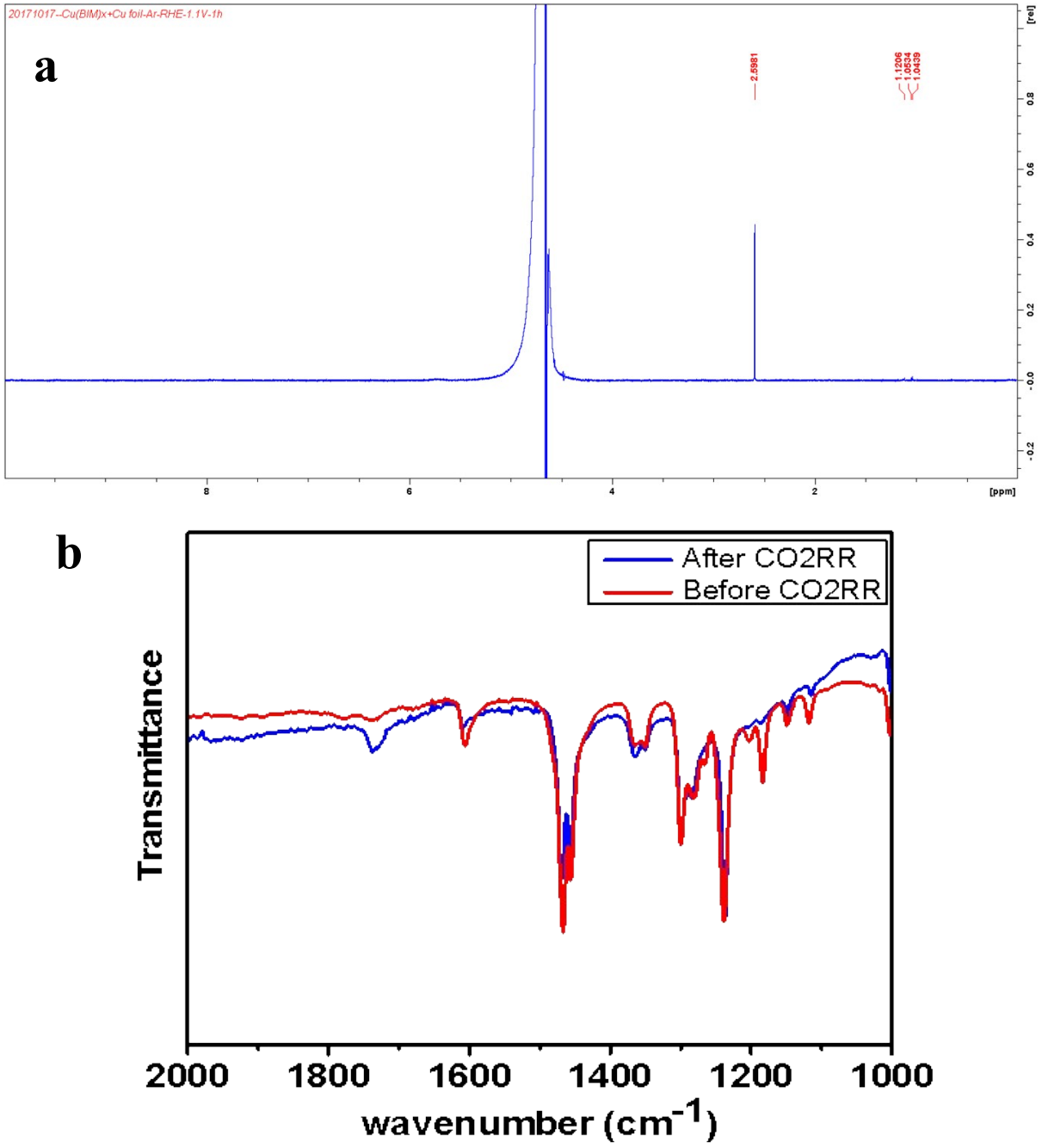

Figure S10 | a. Cu(BIM)$_x$ modified Cu foil was electrolyzed in 0.1 M $KHCO_3$ with a flow of Ar under -1.1 V (vs. RHE) for 1h, no carbon containing products being detected. b. FT-IR of Cu(BIM)x modified Cu foil before and after CO_2RR at -1.07 V vs. RHE. Similar peak information prove the stable of Cu(BIM)x complexes.

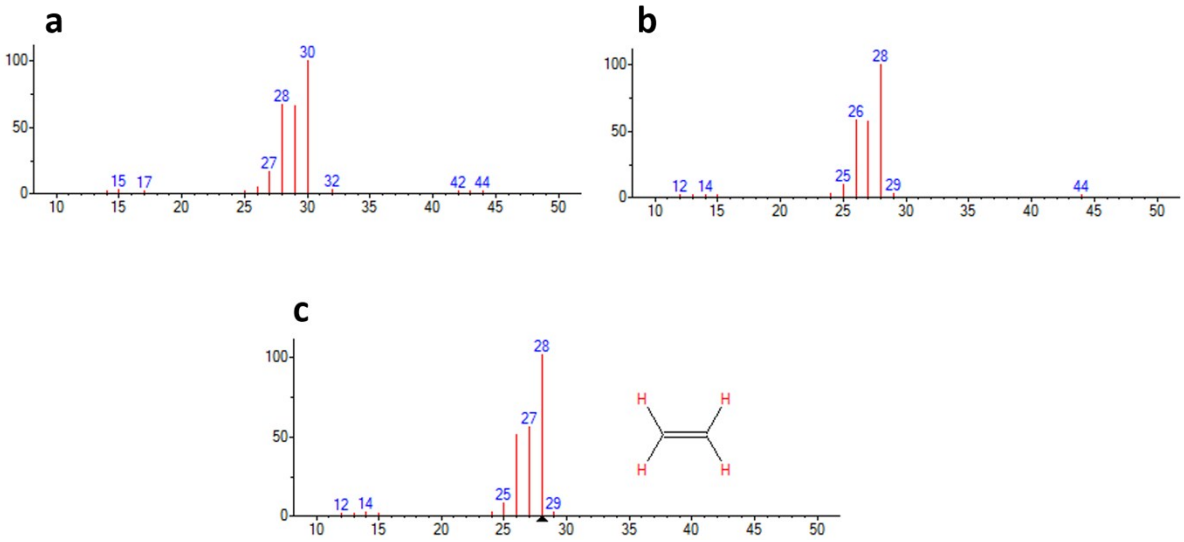

Figure S11 | C_2H_4 produced in $^{13}CO_2$ (a) and $^{12}CO_2$ (b) at -1.05 V, $^{12}C_2H_4$ standard reference(c).

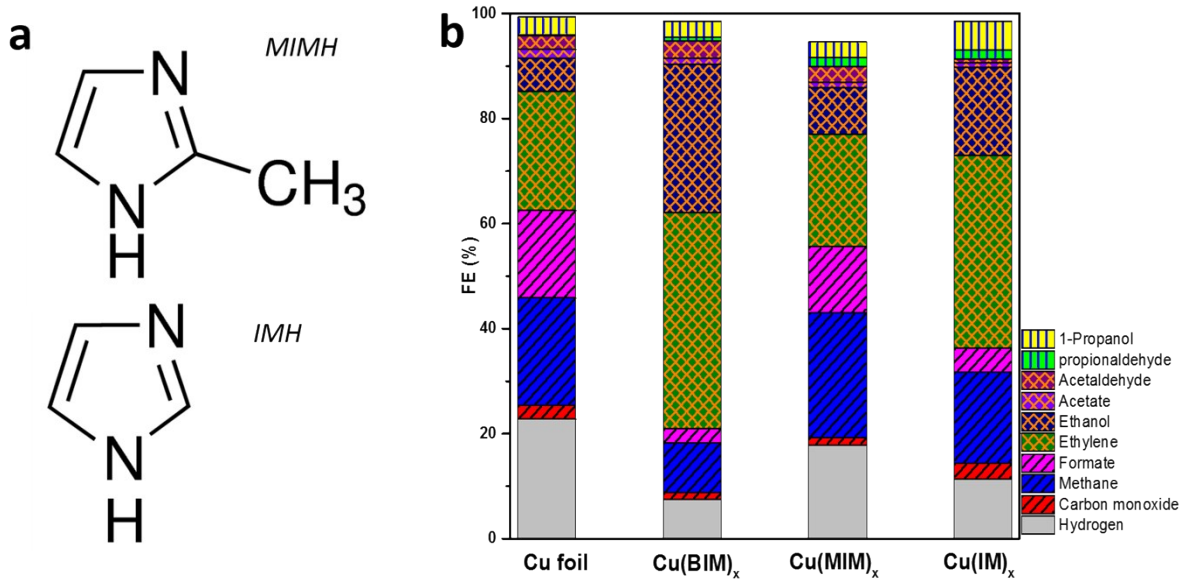

Figure S12 | (a) Molecular structures of two different imidazole ligands, 2-methylimidazole (MIMH) and imidazole (IMH). (b) The catalytic performance of $Cu(IM)_x$ and $Cu(MIM)_x$ modified Cu foil at -1.07 V (vs. RHE).

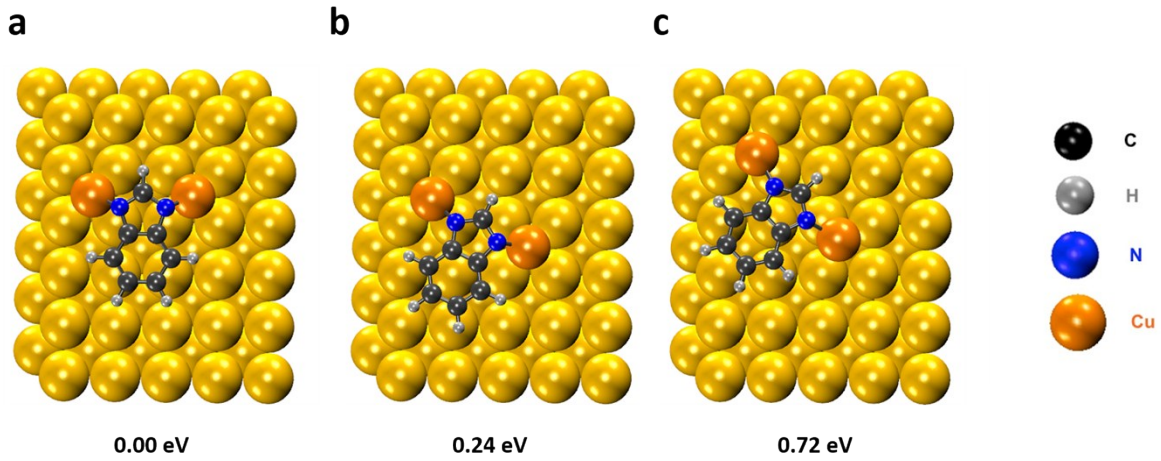

Figure S13 | Relative energy for three possible structures of Cu-coordinated benzimidazole binding on the Cu surface. The first one has the lowest energy, and the following calculations in this paper is based on this structure.

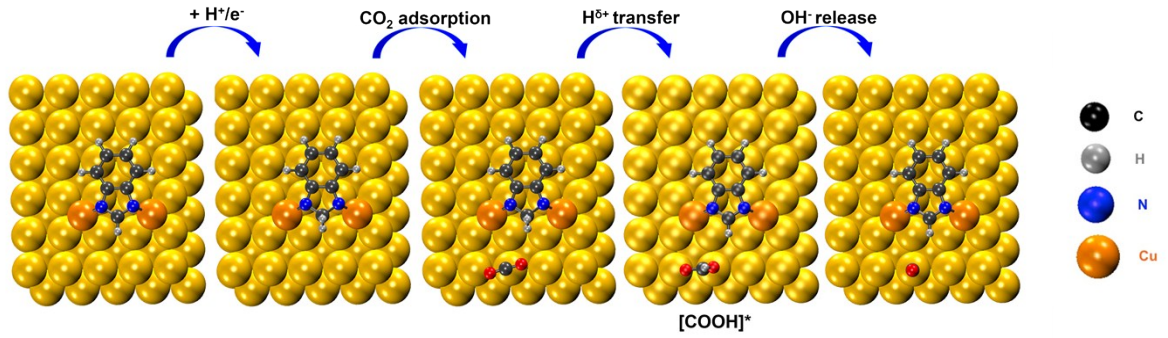

Figure S14 | Schematic representation of CO formation mechanism on Cu(BIM)$_x$ modified Cu foil. The 2-C in the imidazole ring of the BIM adsorbed on Cu surfaces is able to capture partially positive hydrogen ($H^{\delta+}$) and then release it to the adjacently adsorbed CO_2 to form the [COOH*] intermediate. The intermediate can then release OH^- to complete the reduction of carbon dioxide to CO.

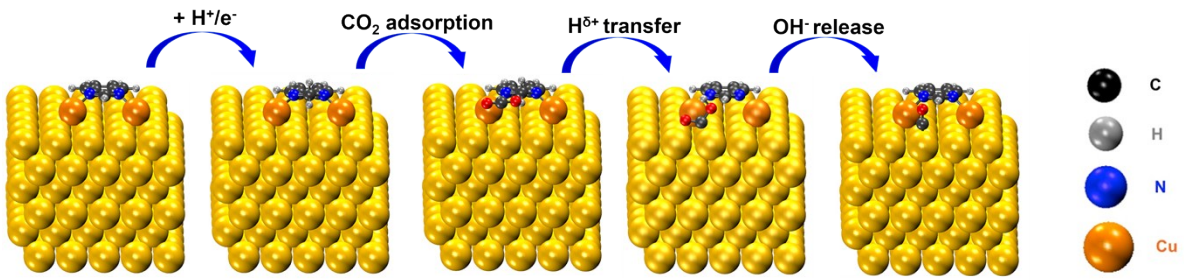

Figure S15 | Side view of schematic representation of CO formation mechanism on $Cu(BIM)_x$ modified Cu foil.

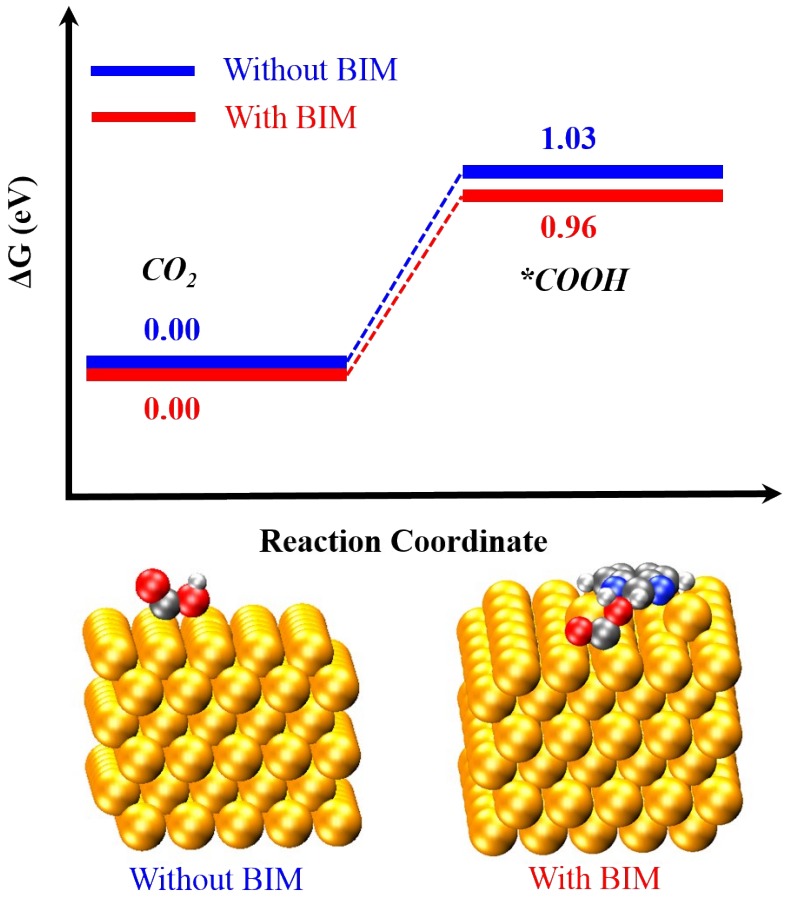

Figure S16 | Free energy diagrams for CO_2 reduction to *COOH intermediate on (100) facet of Cu at -1.07 V vs. RHE.

Reference:

1. Perdew, J. P., Burke, K. & Ernzerhof, M. Generalized gradient approximation made simple. *Phys. Rev. Lett.* **77,** 3865–3868 (1996).

2. Grimme, S., Antony, J., Ehrlich, S. & Krieg, H. A consistent and accurate ab initio parametrization of density functional dispersion correction (DFT-D) for the 94 elements H-Pu. *J. Chem. Phys.* **132,** 154104 (2010).

3. Kresse, G. & Joubert, D. From ultrasoft pseudopotentials to the projector augmented-wave method. *Phys. Rev. B* **59,** 1758–1775 (1999).

4. Jain, A. *et al.* Commentary: The materials project: A materials genome approach to accelerating materials innovation. *APL Mater.* **1,** (2013).

5. Cheng, T., Xiao, H. & Goddard, W. A. Reaction Mechanisms for the Electrochemical Reduction of CO_2 to CO and Formate on the Cu(100) Surface at 298 K from Quantum Mechanics Free Energy Calculations with Explicit Water. *J. Am. Chem. Soc.* **138,** 13802–13805 (2016).

6. Peterson, A. A., Abild-Pedersen, F., Studt, F., Rossmeisl, J. & Nørskov, J. K. How copper catalyzes the electroreduction of carbon dioxide into hydrocarbon fuels. *Energy Environ. Sci.* **3,** 1311 (2010).

7. Xiao, H., Cheng, T., Goddard, W. A. & Sundararaman, R. Mechanistic Explanation of the pH Dependence and Onset Potentials for Hydrocarbon Products from Electrochemical Reduction of CO on Cu (111). *J. Am. Chem. Soc.* **138,** 483–486 (2016).

8. Suffren, Y., Rollet, F. & Reber, C. in *Comments on inorganic chemistry : a journal of critical discussion of the current literature* 246–276 (2011).

9. Kuhl, K. P., Cave, E. R., Abram, D. N. & Jaramillo, T. F. New insights into the electrochemical reduction of carbon dioxide on metallic copper surfaces. *Energy Environ. Sci.* **5,** 7050–7059 (2012).